Research Paper

Properties and Bifunctional Catalytic Activity of Niobium-Doped Silica-Titania: Effect of Phosphoric Acid Treatment

Siew Ling Lee[1]*, Jamilah Mohd Ekhsan[1], Chui Min Ling[2]

[1]*Center for Sustainable Nanomaterials, Ibnu Sina Institute for Scientific and Industrial Research, Universiti Teknologi Malaysia, Johor, 81310, Malaysia*
[2]*Chemistry Department, Faculty of Science, Universiti Teknologi Malaysia, Johor, 81310, Malaysia*
Corresponding author: lsling@utm.my

Abstract

The effect of phosphoric acid treatment on the physical-chemical properties and catalytic activity of the niobium-doped silica-titania bifunctional catalyst was investigated. As part of the synthesis procedure to produce xPO$_4^-$/Nb/TiO$_2$-SiO$_2$, different concentrations of phosphoric acid (H$_3$PO$_4$) were used (x= 0, 0.05, 0.10, 0.15, 0.20, 0.25 M). As shown by XRD analysis, the samples synthesized using 0–0.20 M H$_3$PO$_4$ were in amorphous form, as featureless diffractograms were obtained, indicating the PO$_4^-$ groups were dispersed homogeneously on the surface of Nb doped SiO$_2$-TiO$_2$. Due to the increased concentration of acid, other compounds were formed in the samples by reactions between PO$_4^-$ and Nb and/or Ti. Additionally, UV-Vis DRS results indicated that the presence of the PO$_4^-$ group accelerated the transformation of hydrated tetrahedral Ti species into isolated tetrahedral Ti species. An experimental investigation of the catalytic performance of the catalyst was conducted using 1,2-epoxyoctane as an oxidant for the epoxidation of 1-octene to 1,2-octanediol. It has been demonstrated that H$_3$PO$_4$ treatment was essential for oxidative and acidity active site formation. The current research findings strongly suggested that Nb-doped TiO$_2$-SiO$_2$ treated with 0.2 M H$_3$PO$_4$ was the most effective bifunctional catalyst in generating 1,2-octanediol.

Keywords

Phosphoric Acid, Oxidative, Brønsted Acid, Titania, Niobium, Silica

1. INTRODUCTION

A diol is a valuable feedstock in the fine chemical industry and a key intermediate in the synthesis of fragrances, pesticides, and pharmaceuticals (Alphy et al., 2021). In the present process, diols are formed via two steps, first by oxidizing alkene to epoxy and then by reacting epoxy with an acidic catalyst to yield diol. Consequently, it has resulted in a labor-intensive, time-consuming, and inefficient process as two reactors are needed. It is therefore highly desirable to develop bifunctional catalysts which contain two different active sites in one material.

The acidic catalysts have been widely used in many kinds of chemical reactions (Mulyatun et al., 2021; Munyentwali et al., 2022). Anionic metal oxides containing sulphates, tungstates, and phosphates, which exhibit a high affinity for acid-catalyzed reactions, have recently received attention in heterogeneous catalysis (Sosa et al., 2022; Lim and Lee, 2016; Lee et al., 2015). Solid acids, also important heterogeneous catalysts, can be utilized in many applications such as hydrocarbon cracking, alkane isomerization, and valorization of biomass. The catalytic activity of the solid acids is greatly influenced by the na-

ture of acid sites due to the presence of Brønsted and Lewis acidity (Ekhsan et al., 2014). It was claimed that the co-existence of Brønsted and Lewis acid sites has improved the acidity of the solid catalysts.

For the last two decades, titanium dioxide or titania (TiO$_2$) and TiO$_2$-based heterogeneous catalysts have been intensively investigated for diol production (Wada et al., 2017; Lee and Hamdan, 2008). In fact, these materials have been widely applied as effective catalysts in pollutant removal, the pigment in paint products, and oxidation reactions (Koh et al., 2017; Chen et al., 2022; Ling et al., 2020; Leong et al., 2022). It was documented that TS-1, a TiO$_2$-containing silicalite was a promising oxidative catalyst attributed to the presence of tetrahedrally coordinated titanium in a silicate structure (Zhao et al., 2022). However, only Lewis acidity was found in TiO$_2$-SiO$_2$ mixed oxides, without any Brønsted acidity (Wu et al., 2021).

It had been demonstrated that acid treatment increased the acidity of the designed catalysts (Lim and Lee, 2016; Lee and Hamdan, 2008). Both Lewis and Brønsted acidic sites

were generated in titania and alumina upon loading of phosphoric acid (Ortiz-Islas et al., 2005). In addition, silica treated with phosphoric acid showed high Brønsted acidity (Kahraman et al., 2005). In other work, the interaction between vanadia and phosphate was claimed to be important for the Brønsted acid site formation in a titanium-silica bifunctional catalyst. The presence of phosphoric acid was also important in strengthening the oxidative catalytic activity of the catalysts.

Previous studies reported that iron phosphate ($FePO_4$) was an ideal catalyst for oxidation reactions because it possessed both redox and acidic properties. This oxidative dehydrogenation proved to be particularly selective for $FePO_4$. Despite this, this material did not have a high oxidation catalytic activity (Tan et al., 2016). The coordinated titania and niobium species, which were tetrahedrally coordinated, are also important components of good catalysts that act as oxidative sites. In Nb-impregnated TS-1 catalysts, the presence of niobium compound led to Brønsted acidity formation and sufficient diol production (Ahn et al., 2020).

Thus, here, we present the preparation of a series of phosphoric acid-treated niobium-doped titania-silica. The effect of the phosphate treatment on the physical-chemical properties of the resulting material was investigated. The importance of the phosphor acid as a modifier of niobium-doped titania-silica bifunctional was examined. Furthermore, the catalytic performance of the synthesized materials was examined in the sequential transformation of 1-octene into 1,2-octanediol by forming 1,2-epoxyoctane.

2. EXPERIMENTAL SECTION

2.1 Synthesis of Materials

Using the sol-gel and impregnation techniques, phosphoric acid concentrations were prepared on modified niobium (Nb) titania-silica (TiO_2-SiO_2). To achieve this purpose, a series of solutions of PO_4^- treated Nb/TiO_2-SiO_2 materials were prepared. Using tetraethylorthosilicate and titanium(IV) isopropoxide, respectively, as SiO_2 and TiO_2 sources, the catalyst support of Si:Ti= 30:1 molar ratio was prepared using the sol-gel method according to previously reported methods (Ekhsan et al., 2014). After stirring TEOS, ethanol, HNO_3, and H_2O (mol ratios 1: 1: 0.6: 4) for 30 minutes at room temperature, a solution of these components was obtained. Titanium(IV) isopropoxide (TTIP, Aldrich, 97%), acetylacetone and ethanol (mol ratio= 1: 0.5: 100) were added to the mixture and stirred at room temperature for 30 minutes. After stirring the clear solution for 1 hour, the mixture was dried at 80°C to get a clear gel. Following the drying of the wet gel at 110°C overnight, it was calcined at 500°C for 5 hours to produce SiO_2-TiO_2 powder.

As a part of the impregnation process, 1.8 g of SiO_2-TiO_2 was added to the niobium solution. At this stage, 1 wt% of niobium(V) ethoxide was prepared by dissolving it in sufficient amounts of niobium(V) ethoxide ($Nb(OC_2H_5)_5$) (Aldrich, 99.95%) in 10 mL of n-hexane. A stirring process at room temperature was followed by overnight drying at 110°C and

stirring at room temperature. During the calcination process, the powder was ground and calcined at 500°C for five hours. The material produced was labeled as Nb/SiO_2-TiO_2.

The phosphoric acid of different molarity was used for the further modification of the catalysts via the wet impregnation method. The final products were labeled as xPO_4^-/Nb/SiO_2-TiO_2, where x= 0.05-0.25 M. All the synthesized catalysts were labeled for each sample based on the concentration of phosphoric acid it contains, for example, 0.05PO_4^-/Nb/SiO_2-TiO_2 for 0.05 M H_3PO_4 treated Nb/SiO_2-TiO_2 sample.

2.2 Characterizations

For the determination of the surface area of all samples, Micromeritics ASAP2010 surface area analyzer was used to conduct BET N_2 adsorption-desorption on each sample. Al_2O_3 was used as the standard material to calibrate the analyzer prior to analysis. The crystalline phase of the catalysts was examined using powder X-Ray Diffraction (XRD). The XRD analysis was performed at 40 kV and 40 mA, using a Bruker Advance D8 equipped with Siemens 5000 diffractometer, with Cu Kα radiation (λ = 1.5405 Å) as the diffracted monochromatic beam. Scans of the spectra were performed in the range 2θ of 2°-60° at a step of 0.030° and a time step of 1 s. In addition, infrared measurements were conducted on a Perkin Elmer Spectrum One FT-IR spectrometer via the KBr pellet technique, with a scan time of 10 s and spectral resolution of 2 cm^{-1}. Diffuse reflectance UV spectra were collected to determine Ti and Nb species that existed in the samples. With a Perkin Elmer Lambda 900 DRUV/VIS spectrometer, the analysis was performed under ambient conditions over a range of 190 to 800 nm.

2.3 Catalytic Testing

In order to evaluate the bifunctional catalytic properties of the synthesized samples, the sequential reaction of generation of 1,2-octanediol via the conversion of 1,2-epoxyoctane from 1-octene was followed. The chemical reaction is shown in Figure 1.
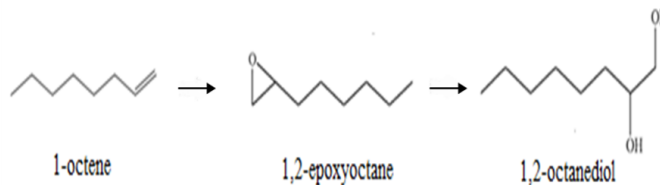

Figure 1. Formation of 1,2-octanediol from 1-octene Through 1,2-epoxyoctane Generation

For this purpose, 1-octene (15 mmol, Aldrich, 98%), 30 mmol hydrogen peroxide in H_2O (Qrec, 30%), and acetonitrile (10 mL, Merck, 99.8%) as solvent were added into a flask equipped with a magnetic stirrer and a condenser. Besides, 250 μL cyclooctane (Fluka, 99%) as the internal standard was out into the flask. The solution was then treated with 0.05 g

catalyst. The reaction was conducted in an oil bath at 70°C for 24 hours with stirring. Finally, the reaction products were analyzed using an HP Agilent 6890N gas chromatograph with an Ultra-1 column.

3. RESULT AND DISCUSSSION

3.1 Properties of Materials

All the prepared materials existed in light white and fluffy powder despite calcination at 500°C for 5 hours. XRD patterns of all the PO_4^-/Nb/SiO_2-TiO_2 samples are shown in Figure 2. As can be observed, the samples Nb/SiO_2-TiO_2 and those treated with 0.20 M or less H_3PO_4 did not exhibit any peaks in the X-ray diffractograms, strongly suggesting that they were amorphous. An H_3PO_4 treatment has been claimed to facilitate well dispersion of Nb on catalyst supports (Onoda and Matsukura, 2015). The amorphous nature of the samples could be also due to the small amount of both TiO_2 and Nb in the samples. As for sample $0.25PO_4^-$/Nb/SiO_2-TiO_2, its XRD diffractogram included some unidentified peaks. The phenomenon might be explained by the possible reactions of H_3PO_4 with Nb and Ti, which generated other compounds in the material. Since impurities are present in $0.25PO_4^-$/Nb/SiO_2-TiO_2, this material was not further characterized and tested for catalytic behavior.
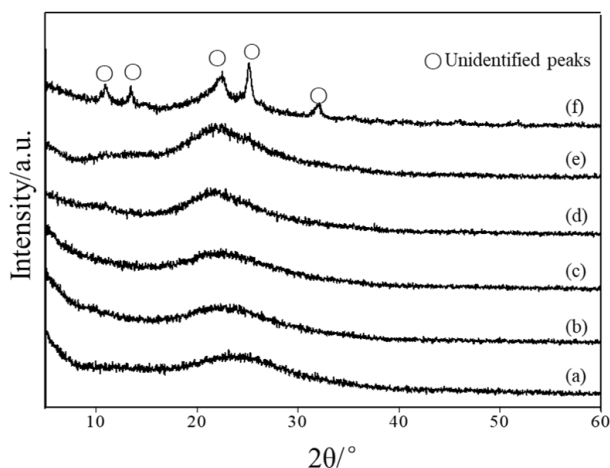

Figure 2. X-Ray Diffractograms of Materials (a) Nb/SiO_2-TiO_2, (b) $0.05PO_4^-$/Nb/SiO_2-TiO_2, (c) $0.10PO_4^-$/Nb/SiO_2-TiO_2, (d) $0.15PO_4^-$/Nb/SiO_2-TiO_2, (e) $0.20PO_4^-$/Nb/SiO_2-TiO_2 and (f) $0.25PO_4^-$/Nb/SiO_2-TiO_2

According to Table 1, both the surface area and pores volume of the materials are reduced upon the addition of Nb and PO_4^-. As a result of using 0.15 and 0.20 M H_3PO_4 in the synthesis of the catalyst, a reduction of ~90% in surface area was detected. As a result of the use of phosphoric acid, the materials exhibited a coalescence process during the calcinations, leading to a drastic decrease in both surface area and pore volume (Lee et al., 2011). A similar phenomenon was also observed on $FePO_4$/SiO_2 catalysts (Ebert et al., 2017).

Table 1. Surface Area and Pore Volume of xPO4-/Nb/SiO_2-TiO_2 Materials

Materials	Surface Area (m^2/g)	Pore Volume (cm^3/g)
SiO_2	572	0.32
Nb/SiO_2-TiO_2	602	0.37
$0.05PO_4^-$/Nb/SiO_2-TiO_2	350	0.23
$0.10PO_4^-$/Nb/SiO_2-TiO_2	300	0.19
$0.15PO_4^-$/Nb/SiO_2-TiO_2	32	0.11
$0.20PO_4^-$/Nb/SiO_2-TiO_2	38	0.12

The FTIR analysis of the resulting materials revealed different functional groups, as shown in Figure 3. As can be seen in all spectra, the characteristic vibration bands of SiO_2 were detected at 466 and 1100 cm^{-1}, corresponding to the bending and stretching vibrations of Si-O-Si, respectively (Ling et al., 2020). Additionally, the weak band at 2341 cm^{-1} was attributed to the presence of Nb. The bands at 1651 and 3400 cm^{-1} were associated with stretching of the O-H atoms and water hydration, respectively. It has been observed that as the concentration of PO_4^- in the sample increased, the intensity of the O-H group decreased. There may be an explanation for this by replacing the O-H group on the surface of the samples with the PO_4^- group. However, no bands were observed corresponding to H_3PO_4. Perhaps this was caused by the low concentration of H_3PO_4 applied in the synthesis process.
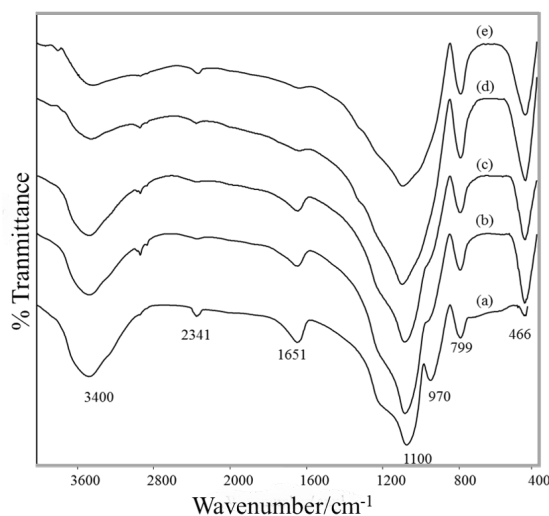

Figure 3. FTIR Spectra of Materials (a) Nb/SiO_2-TiO_2, (b) $0.05PO_4^-$/Nb/SiO_2-TiO_2, (c) $0.10PO_4^-$/Nb/SiO_2-TiO_2, (d) $0.15PO_4^-$/Nb/SiO_2-TiO_2, (e) $0.20PO_4^-$/Nb/SiO_2-TiO_2

A Si-O-Ti bond was observed in all spectra at 799 cm^{-1}, as depicted in Figure 3. Similarly, the band at ~970 cm^{-1} may overlap absorptions of the Si-O-Ti bond, also related to tetrahedral Ti, and be connected to surface Si-OH vibrations.

Interestingly, the band appeared to disappear when the concentration of H_3PO_4 was high. For the PO_4^- treated Nb/SiO_2-TiO_2 samples, only a weak shoulder was observed at ~1000 cm^{-1}. According to this finding, there is a dramatic reduction in Si-O-Ti and Si-O-Si bonding in SiO_2-TiO_2, following H_3PO_4 treatment. It has been described that a small band around 970 cm^{-1} is a result of the interaction between Si-O-M within the silicalite structure (Vicentini et al., 2021). Despite adding Nb, a transition metal to the samples, an additional peak was not observed at this wavenumber. There could be an explanation for this phenomenon in the overlapping with the Si-OH stretching peak, which made it difficult to identify the band precisely (Lee et al., 2011).

Figure 4 illustrates the UV-Vis DRS spectra for the xPO_4^-/Nb/SiO_2-TiO_2. There was an intense band present at 270 nm for all materials. The band corresponds to the hydrated tetrahedral Ti species found in the samples. Observably, the intensity of this band increased as the amount of PO_4^- used increased.
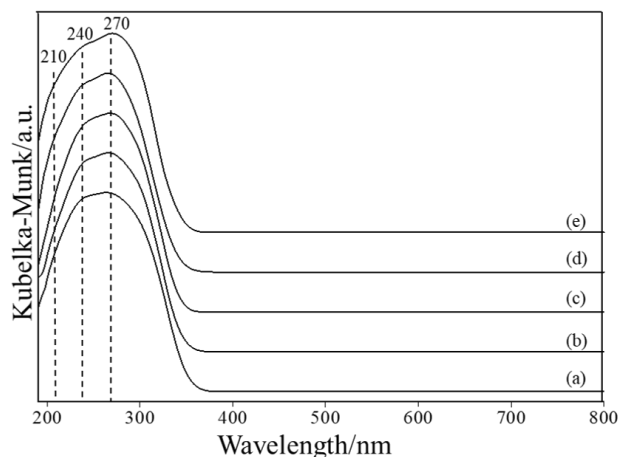

Figure 4. UV-Vis Spectra of Materials (a) Nb/SiO_2-TiO_2, (b) $0.05PO_4^-$/Nb/SiO_2-TiO_2, (c) $0.10PO_4^-$/Nb/SiO_2-TiO_2, (d) $0.15PO_4^-$/Nb/SiO_2-TiO_2 and (e) $0.20PO_4^-$/Nb/SiO_2-TiO_2

Based on the fact that the H_3PO_4 modified samples are more hydrophilic, the hydration of tetrahedral Ti species has been facilitated. Therefore, it was determined that the $0.20PO_4^-$/Nb-TiO_2-SiO_2 sample was more hydrophilic than other prepared samples as proven in the FTIR spectra of the samples (Figure 3). Similar results were noted when V and PO_4^- groups were present on the surface of the SiO_2 support, increasing the amount of hydrated tetrahedral Ti species (Lee et al., 2009). In spite of the amorphous nature of the samples, continuity of tetrahedrally coordinated silicate polymer chains was observed for the Ti species in H_3PO_4 modified Nb-impregnated SiO_2-TiO_2.

Meanwhile, impregnation of Nb onto SiO_2-TiO_2 produced a band at around 240 nm that was due to octahedral Nb species

(Tiozzo et al., 2013). In addition, the small band at 210 nm was associated with ligand-to-metal charge transfer in tetrahedral coordination, Td, between an O^{2-} atom and a center Ti(IV) atom (Goswami et al., 2013). Accordingly, the SiO_2 matrix contained tetrahedral Ti(IV) ions, which indicates the prevalence of Ti species within the matrix. When H_3PO_4 concentrations were varied, no significant changes were observed in these two bands.

3.2 Catalytic Testing

In this study, the bifunctional catalytic performance of xPO_4^-/Nb/SiO_2-TiO_2 ($x = 0, 0.05, 0.10, 0.15, 0.20$ M) materials was evaluated. In accordance with Table 2, all the PO_4^- treated Nb-modified SiO_2-TiO_2 materials catalyzed the oxidation of 1,2-epoxyoactane. In comparison with the Nb/SiO_2-TiO_2 sample without PO_4^- treatment, the addition of PO_4^- resulted in a significant increase in epoxide yields. It might be interpreted as evidence that the presence of the PO_4^- group strengthens oxidative active sites in the samples. As a result of the oxidative reaction, $0.05PO_4^-$/Nb/SiO_2-TiO_2 proved to be the most efficient catalyst, producing 382 μmol of 1,2-epoxyoctane after 24 hours of reaction.

Table 2. Product Yields of the Materials in Transformation of 1-octene to 1,2-octanediol Through 1,2-epoxyoctane Generation at 343 K for 24 h

Materials	Yield of 1,2-epoxyoctane (μmol)	Yield of 1,2-octanediol (μmol)
Nb/SiO_2-TiO_2	59	0
$0.05PO_4^-$/Nb/SiO_2-TiO_2	382	0
$0.10PO_4^-$/Nb/SiO_2-TiO_2	333	0
$0.15PO_4^-$/Nb/SiO_2-TiO_2	195	0
$0.20PO_4^-$/Nb/SiO_2-TiO_2	164	461

However, 1,2-octanediol was only yielded when $0.20PO_4^-$/Nb/SiO_2-TiO_2 was used as a catalyst in the reaction. It could be observed that $0.20PO_4^-$/Nb/SiO_2-TiO_2 was an effective bifunctional catalyst after 24 hours since it yielded 461 μmol 1,2-octanediol. It was reported previously by our group that $0.20PO_4^-$/Nb/SiO_2-TiO_2 possessed 14.6 μmol/g Lewis acid and 2.4 μmol/g Brønsted acid as confirmed via pyridine adsorption analysis (Ekhsan et al., 2014). Since the existence of Brønsted acid sites in V_PO_4/ST catalysts has been reported to be due to the coexistence of PO_4^- and V compounds (Lee et al., 2009), the interaction between PO_4^- and Nb compounds in the prepared samples could be important to generate the Brønsted acid sites. For samples Nb/SiO_2-TiO_2 treated with lesser amount of H_3PO_4 ($x= 0.05, 0.10, 0.15$ M), no diol was produced. This could be due to the insufficient amount of PO_4^- for the formation of Brønsted acidity with Nb in the samples. As with Nb/TiO_2-SiO_2, Nb/SiO_2-TiO_2 had no Brønsted acid sites, so it was inactive in the epoxide-diol transformation.

4. CONCLUSION

Bifunctional catalysts of PO_4^- treated Nb/SiO_2-TiO_2 were synthesized via sol-gel and impregnation methods. It was observed that the hydrated tetrahedral Ti species present as the most predominant species, and the amount of this Ti species increased with the increase of PO_4^- concentration. After 24 hours of reaction, 0.05 M PO_4^- treated Nb/SiO_2-TiO_2 proved to be the most efficient oxidative catalyst, strongly suggesting the PO_4^- treatment has increased significantly the oxidative active sites in the samples. More importantly, the current results revealed that 0.20 M PO_4^- treated Nb/SiO_2-TiO_2 is a promising bifunctional catalyst for the transformation of 1-octene to 1,2-octanediol through the generation of 1,2-epoxyoactane. The research finding indicated that a sufficient amount of PO_4^- was crucial to generate Brønsted acidity for the transformation of 1,2-epoxides to diol.

5. ACKNOWLEDGMENT

REFERENCES

Ahn, S., S. L. Nauert, K. E. Hicks, M. A. Ardagh, N. M. Schweitzer, O. K. Farha, and J. M. Notestein (2020). Demonstrating the Critical Role of Solvation in Supported Ti and Nb Epoxidation Catalysts Via Vapor-Phase Kinetics. *ACS Catalysis*, **10**(4); 2817–2825

Alphy, M. P., S. H. Hazeena, M. Binoop, A. Madhavan, K. Arun, N. Vivek, R. Sindhu, M. K. Awasthi, and P. Binod (2021). Synthesis of C2-C4 Diols from Bioresources: Pathways and Metabolic Intervention Strategies. *Bioresource Technology*, **346**; 126410

Chen, M. C., P. W. Koh, V. K. Ponnusamy, and S. L. Lee (2022). Titanium Dioxide and Other Nanomaterials Based Antimicrobial Additives in Functional Paints and Coatings. *Progress in Organic Coatings*, **163**; 106660

Ebert, D. Y., A. Savel'eva, N. Dorofeeva, and O. Vodyankina (2017). FePO$_4$/SiO$_2$ Catalysts for Propylene Glycol Oxidation. *Kinetics and Catalysis*, **58**(6); 720–725

Ekhsan, J. M., S. L. Lee, and H. Nur (2014). Niobium Oxide and Phosphoric Acid Impregnated Silica–Titania as Oxidative-Acidic Bifunctional Catalyst. *Applied Catalysis A: General*, **471**; 142–148

Goswami, P., R. K. Debnath, and J. N. Ganguli (2013). Photophysical and Photochemical Properties of Nanosized Cobalt-Doped TiO$_2$ Photocatalyst. *Asian Journal of Chemistry*, **25**(13); 7118–7124

Kahraman, S., M. Önal, Y. Sarıkaya, and İ. Bozdoğan (2005). Characterization of Silica Polymorphs in Kaolins by X-Ray Diffraction Before and After Phosphoric Acid Digestion and Thermal Treatment. *Analytica Chimica Acta*, **552**(1-2); 201–206

Koh, P. W., M. H. M. Hatta, S. T. Ong, L. Yuliati, and S. L. Lee (2017). Photocatalytic Degradation of Photosensitizing and Non-Photosensitizing Dyes Over Chromium Doped Titania Photocatalysts Under Visible Light. *Journal of Photochemistry and Photobiology A: Chemistry*, **332**; 215–223

Lee, S. L., J. M. Ekhsan, N. A. Kasiran, and A. A. Aziz (2015). Effect of Titania Loading on Properties and Catalytic Activity of Nanostructured Phosphate–Vanadia-Impregnated Silica–Titania Oxidative–Acidic Bifunctional Catalyst. *International Journal of Chemical Reactor Engineering*, **13**(1); 21–28

Lee, S. L. and H. Hamdan (2008). Sulfated Silica–Titania Aerogel as a Bifunctional Oxidative and Acidic Catalyst in the Synthesis of Diols. *Journal of Non-Crystalline Solids*, **354**(33); 3939–3943

Lee, S. L., H. Nur, and H. Hamdan (2009). Physical Properties and Bifunctional Catalytic Performance of Phosphate–Vanadium Impregnated Silica–Titania Aerogel. *Catalysis Letters*, **132**(1); 28–33

Lee, S. L., H. Nur, P. W. Koh, J. M. Ekhsan, and S. C. Wei (2011). Synthesis and Characterization of Acid Modified Silica-Titania Aerogel as Oxidative-Acidic Bifunctional Catalyst. *International Journal of Applied Physics and Mathematics*, **1**(1); 43

Leong, C. Y., H. L. Teh, M. C. Chen, and S. L. Lee (2022). Effect of Synthesis Methods on Properties of Copper Oxide Doped Titanium Dioxide Photocatalyst in Dye Photodegradation of Rhodamine B. *Science and Technology Indonesia*, **7**(1); 91–97

Lim, S. E. and S. L. Lee (2016). New Tungsten-Sulphate Modified Silica-Titania as Oxidative-Acidic Bifunctional Catalyst for Diol Formation. *Malaysian Journal of Catalysis*, **1**(1); 17–21

Ling, C. M., L. Yuliati, H. O. Lintang, and S. L. Lee (2020). TUD-C-Supported Tungsten Oxide-Doped Titania Catalysts for Cyclohexane Oxidation. *Malaysian Journal Chemistry*, **22**(2); 29–36

Mulyatun, M., J. Prameswari, I. Istadi, and W. Widayat (2021). Production of Non-Food Feedstock Based Biodiesel Using Acid-Base Bifunctional Heterogeneous Catalysts: a Review. *Fuel*; 122749

Munyentwali, A., H. Li, and Q. Yang (2022). Review of Advances in Bifunctional Solid Acid/Base Catalysts for Sustainable Biodiesel Production. *Applied Catalysis A: General*, **633**; 118525

Onoda, H. and A. Matsukura (2015). Influence of Concentration in Phosphoric Acid Treatment of Titanium Oxide and Their Powder Properties. *Journal of Asian Ceramic Societies*, **3**(1); 27–31

Ortiz-Islas, E., R. Gomez, T. Lopez, J. Navarrete, D. Aguilar, and P. Quintana (2005). Effect of the Crystallite Size in the Structural and Textural Properties of Sulfated and Phosphated Titania. *Applied Surface Science*, **252**(3); 807–812

Sosa, A. A., V. Palermo, P. Langer, R. Luque, G. P. Romanelli, and L. R. Pizzio (2022). Tungstophosphoric Acid/Mesoporous Silicas as Suitable Catalysts in Quinoxa-

line Synthesis. *Molecular Catalysis*, **517**; 112046

Tan, S., B. Hu, W. G. Kim, S. H. Pang, J. S. Moore, Y. Liu, R. S. Dixit, J. G. Pendergast, D. S. Sholl, and S. Nair (2016). Propane Dehydrogenation Over Alumina-Supported Iron/Phosphorus Catalysts: Structural Evolution of Iron Species Leading to High Activity and Propylene Selectivity. *ACS Catalysis*, **6**(9); 5673–5683

Tiozzo, C., C. Bisio, F. Carniato, A. Gallo, S. L. Scott, R. Psaro, and M. Guidotti (2013). Niobium–Silica Catalysts for the Selective Epoxidation of Cyclic Alkenes: the Generation of the Active Site by Grafting Niobocene Dichloride. *Physical Chemistry Chemical Physics*, **15**(32); 13354–13362

Vicentini, J. C. M., R. Manieri, G. W. Subtil, F. de Oliveira Tavares, D. M. de Oliveira, P. H. Yassue-Cordeiro, H. Enzweiler, M. L. Gimenes, M. d. C. M. Alves, and J. Morais (2021). Photocatalytic Water Splitting with Noble-Metal Free Cocatalysts for a Comprehensive Study of Two Nonidentical Photoreactors Designs. *Environmental Progress and Sustainable Energy*, **40**(3); e13557

Wada, E., A. Tyagi, A. Yamamoto, and H. Yoshida (2017). Dehydrogenative Lactonization of Diols with a Platinum-Loaded Titanium Oxide Photocatalyst. *Photochemical and Photobiological Sciences*, **16**(12); 1744–1748

Wu, W., D. T. Tran, S. Cheng, Y. Zhang, N. Li, H. Chen, Y. H. C. Chin, L. Yao, and D. Liu (2021). Local Environment and Catalytic Property of External Lewis Acid Sites in Hierarchical Lamellar Titanium Silicalite-1 Zeolites. *Microporous and Mesoporous Materials*, **311**; 110710

Zhao, P., Z. Li, Y. Zhang, D. Cui, Q. Guo, Z. Dong, G. Qi, J. Xu, and F. Deng (2022). Tuning Lewis Acid Sites in TS-1 Zeolites for Hydroxylation of Anisole with Hydrogen Peroxide. *Microporous and Mesoporous Materials*, **335**; 111840